

Evidence of magnetic star-planet interactions in the HD 189733 system from orbitally-phased Ca II K variations

P. WILSON CAULEY,¹ EVGENYA L. SHKOLNIK,¹ JOE LLAMA,² VINCENT BOURRIER,³ AND CLAIRE MOUTOU⁴

¹*Arizona State University, School of Earth and Space Exploration, Tempe, AZ 85287*

²*Lowell Observatory, Flagstaff, AZ 86001*

³*Observatoire de l'Université de Genève, 1290 Sauverny, Switzerland*

⁴*CFHT Corporation, Kamuela, HA 96743*

(Received 9/10/18; Accepted 10/10/18)

Submitted to AJ

ABSTRACT

Magnetic star-planet interactions (SPI) provide a detection method and insight into exoplanet magnetic fields and, in turn, exoplanet interiors and atmospheric environments. These signatures can be sporadic and difficult to confirm for single-epoch observations of a system due to inhomogeneous stellar magnetospheres and periodic variability in stellar magnetism. Thus an ideal SPI search consists of multiple epochs containing observations on consecutive nights spanning at least one complete planetary orbit. Such data sets are rare but do exist for some of the most intensely studied hot Jupiter systems. One such system is HD 189733 for which six suitable SPI data sets exist, the result of spectroscopic monitoring to perform some of the first SPI searches and also to study the star's magnetic field. Here we perform a uniform analysis of six archival Ca II K data sets for HD 189733, spanning 2006 June through 2015 July, in order to search for magnetic SPI signatures in the chromospheric line variations. We find significant evidence for modulations of Ca II K with a 2.29 ± 0.04 day period in the 2013 August data, which is consistent with the planet's orbital period. The peak in the orbital variations occurs at $\phi_{\text{orb}} \approx 0.9$, which corresponds to the SPI emission leading the planet with a phase difference of $\Delta\phi \approx 40^\circ$ from the sub-planetary point. This is consistent with the phase lead predictions of non-linear force-free magnetic field SPI models. The stellar magnetic field strength at the planet's orbit is greatest in 2013 August which, due to the energy released in magnetic SPI scaling with B_* , lends strength to the SPI interpretation.

1. INTRODUCTION

Close-in massive planets, i.e., those with $M_p \gtrsim 0.5M_J$ and $a_{\text{orb}} \lesssim 10R_*$, are capable of strongly interacting with their host stars via tides or reconnection processes involving the magnetospheres of both objects (e.g., Cuntz et al. 2000; Cranmer & Saar 2007; Lanza 2009; Shkolnik & Llama 2017), potentially enhancing the activity level of the host star and affecting the spin evolution of the star and orbital evolution of the planet (Lanza 2010; Cohen et al. 2011; Strugarek et al. 2015). Magnetic star-planet interactions, or SPI, can reveal information about exoplanetary atmospheres and interiors through the detection of magnetic fields (e.g., Lanza 2009; Lazio et al. 2016), characteristics which are difficult to probe and about which we currently have limited knowledge.

HD 189733 b is one of the most well-studied hot Jupiters due to its host star's brightness, high activity level, and a favorable $(R_p/R_*)^2$ for atmospheric characterization (Bouchy et al. 2005). A variety of experiments have been performed searching for SPI signatures in the system. Shkolnik et al. (2008) presented evidence for variability in the Ca II H and K lines as a function of the planet's orbital period, a typical manifestation of magnetic SPI (Shkolnik et al. 2003, 2005). Similar variations were searched for in Fares et al. (2010) across two epochs of ≈ 20 nights each. They found no clear evidence for a SPI signal at the planet's orbital period. Pillitteri et al. (2011), Pillitteri et al. (2014), and Pillitteri et al. (2015) presented evidence of X-ray and UV flares associated with a narrow range of planetary orbital phase, evidence of magnetic SPI between the stellar corona and planetary magnetic field or, in the case of the UV flares, accreting planetary material onto the stellar surface. Poppenhaeger & Wolk (2014) looked at X-ray emission from both HD 189733 A, the planet host, and HD 189733 B, a distant M4V companion, and found that HD 189733 A's X-ray flux suggested a younger age

than its companion. They surmised that the enhanced X-ray flux and fast rotation is a result of stellar spin-up by HD 189733 b. Finally, [Cauley et al. \(2017a\)](#) demonstrated that the H α line core flux surrounding the planetary transit showed abnormal variations compared with times far from transit, suggestive of either SPI or absorption by circumplanetary material.

Magnetic SPI signals can be sporadic: changes in the relative orientation of the stellar and planetary magnetic fields, as well as longer term variability in the stellar magnetic field strength and topology, can cause the SPI mechanism to turn on and off over orbital and stellar activity cycles ([Lanza 2010](#); [Cohen et al. 2011](#); [Strugarek et al. 2015](#)). Furthermore, stochastic changes in stellar activity, which are common for active stars such as HD 189733, unrelated to the planet can contaminate night-to-night signatures, potentially masking phased SPI emission or even resulting in such a signal. Stochastic variability can be tested as the culprit of orbitally phased emission by producing random light curves at the observed phases and calculating the probability of measuring the real signal. This highlights the need for observations which span multiple planetary orbits and, ideally, stellar activity cycles and statistically testing any orbitally phased variability.

In the past decade, numerous observing campaigns have been executed with the purpose of mapping the magnetic field strength and topology of HD 189733 A ([Fares et al. 2010, 2017](#)), as well as a four night SPI investigation by [Shkolnik et al. \(2008\)](#). These data are ideally formatted to search for SPI signals: high signal-to-noise Ca II H and K spectra obtained regularly across multiple planetary orbits. In this paper we present a uniform search for SPI signals in these archival Ca II K spectra of HD 189733. The data consist of six observing runs each containing at least 8 nights, a duration of time which spans ≥ 3 orbital periods of HD 189733 b ($P_{\text{orb}} = 2.2$ days). Although previously analyzed for SPI, we include the data sets from [Fares et al. \(2010\)](#) for completeness and to apply a consistent analysis. [Section 2](#) details the observations and summarizes the data reduction, including steps taken to produce the residual flux spectra used in the SPI analysis. The results are laid out in [Section 3](#) and discussed in [Section 4](#). A brief summary of our conclusions are presented in [Section 5](#).

2. OBSERVATIONS AND DATA REDUCTION

We have re-purposed archived high resolution high-quality spectroscopy of the HD 189733 hot Jupiter system. The selected epochs are detailed in [Table 1](#). All of the data were taken from the PolarBase archive ([Petit et al. 2014](#)). The spectra were reduced using the automated pipeline `libre-esprit`, fully described in [Donati et al. \(1997\)](#) and to which we refer the reader for details. Briefly, each exposure is bias subtracted and flat fielded to remove pixel-to-pixel variations. Inter-order scattered light is then approximated and removed. The

spectra are optimally extracted and a wavelength solution is computed using Th-Ar comparison exposures. The normalized pipeline-reduced spectra are then corrected for heliocentric velocities and small wavelength shifts between spectra are adjusted via a χ^2 comparison of narrow spectral lines in the Ca II H and K order.

The optimal strategy for detecting SPI signatures as a function of planetary orbital phase is to repeatedly observe the host star on consecutive nights across at least two full orbital periods. For this reason, we require that an epoch of observations contains ≥ 5 exposures taken across at least two full planetary orbits. Sparsely sampled portions of observing runs are excluded in favor of stretches with continuous data or that only contain gaps less than or similar to a single orbital period. This can help mitigate contamination from changing stellar activity levels that are not related to rotational modulation. For example, we exclude the first four nights of the full 2007 June data set and the first night of the 2008 July data set due to sparse sampling and their separation from the more densely sampled portions. All of the epochs consist of consecutive observations, with the one exception for 2007 June noted in [Table 1](#).

Individual nightly spectra are examined for quality and rejected if the standard deviation of the residual intra-night flux of the spectrum, measured outside of the Ca II K line core, is $> 1.5\times$ the mean residual flux standard deviation for that night. We do not include an analysis of Ca II H since it correlates directly with Ca II K and is the weaker member of the doublet.

2.1. Preparation of the spectra for SPI analysis

Here we explicitly lay out the steps taken to produce the residual Ca II K fluxes, which is the data product used in the SPI analysis. The individual steps taken, which are illustrated in [Figure 1](#), are as follows:

1. Precise normalization of the Ca II K line core was done using a linear fit to the 0.2 Å on either end of a 6 Å range centered on 3933.66 Å
2. The median was taken of the normalized spectra for each night
3. The mean of the nightly median spectra was taken to create an average Ca II K spectrum for the epoch
4. The mean spectrum was subtracted from each night's median to create residual Ca II K profiles for each night
5. Small offsets in the residual profiles were corrected using a low-order spline fit to points outside of the central 1 Å in the line core
6. The flux were summed across the central 1 Å to produce the residual Ca II K flux for that night

Table 1. Observations of HD 189733

Observation epoch	UT start	UT end	N_{nights}	Instrument	Telescope	$\lambda/\Delta\lambda$	References
(1)	(2)	(3)	(4)	(5)	(6)	(7)	(8)
2006 Jun ^a	2006 Jun 10	2006 Jun 13	4	ESPaDOs	CFHT	65,000	Moutou et al. (2007)
	2006 Jun 16	2006 Jun 19	4	ESPaDOs	CFHT	80,000	Shkolnik et al. (2008)
2007 Jun ^b	2007 Jun 23	2007 Jul 4	8	ESPaDOs	CFHT	65,000	Fares et al. (2010)
2008 Jul	2008 Jul 15	2008 Jul 24	8	NARVAL	TBL	65,000	Fares et al. (2013)
2013 Aug	2013 Aug 4	2013 Aug 22	11	NARVAL	TBL	65,000	Fares et al. (2017)
2013 Sep	2013 Sep 2	2013 Sep 24	13	NARVAL	TBL	65,000	Fares et al. (2017)
2015 Jul	2015 Jul 6	2015 Jul 16	10	NARVAL	TBL	65,000	Fares et al. (2017)

^aThe 2006 June epoch is a combination of two 4-night observing runs. The $R \approx 80,000$ data is convolved with a Gaussian kernel down to $R \approx 65,000$.

^bThe average spectrum from 2007 June 30 is discarded due to low S/N.

7. A sinusoidal function was fit to the residual fluxes to remove variations due to stellar rotation

Each individual spectrum was normalized using a 6 Å region centered on the Ca II K line. A line was then fit to the average of the points comprising 0.2 Å on either end of the 6 Å range (Step 1 in Figure 1). The median of the normalized spectra for each night was taken to produce the median nightly spectrum (Step 2 in Figure 1). The median spectrum was used instead of the mean since intra-night variability is due to stochastic stellar activity, a non-Gaussian process. All median nightly spectra from the epoch were then averaged to create a mean Ca II K profile (Step 3 in Figure 1). Mean spectra are shown in the top row of Figure 2 for each epoch.

Residual profiles for each night were created by subtracting the mean epoch spectrum from the median nightly spectra (Step 4 in Figure 1). Any additional slope or offset in the residual spectrum continuum was subtracted with a low-order spline to points outside of the line core. These offsets were typically $\approx 10\times$ smaller than the peaks of the residual lines cores (e.g., the red line in the middle-left panel of Figure 1). The residual core flux was summed across a 1 Å region centered on the Ca II K rest wavelength (Step 6 in Figure 1). The uncertainty for each flux value in the residual spectrum was set equal to the standard deviation of the spectrum outside of the line core (gray region in the middle panel of Figure 1). The final step was removing variations due to stellar rotation, which is outlined in detail in Section 2.2.

2.2. Removing stellar rotational variations

Before assessing the presence of SPI variations, rotational modulation on the star, if present, must be approximated and removed. HD 189733 is an active star and shows clear rotational variability (e.g., Hébrard et al. 2006; Fares et al. 2010). There is also evidence that HD 189733 is rotating differentially: using the 2007 June data set included here, Fares et al. (2010) measured a

differential rotation rate of $d\Omega = 0.146 \pm 0.049$ radians day^{-1} , which corresponds to an equatorial rotation period of 11.94 ± 0.16 days and a polar rotational period of 16.53 ± 2.43 days. These measurements were confirmed by Fares et al. (2017) who found $d\Omega = 0.11 \pm 0.05$ radians day^{-1} and an equatorial rotational period of 11.7 ± 0.1 days. Cegla et al. (2016) also place a lower limit on the differential rotation value of $d\Omega \geq 0.12$ radians day^{-1} .

We model the rotational variations in the residual Ca II K flux as a sinusoid with a linear trend, letting the period of rotation vary as a free parameter (e.g., Fares et al. 2010). We note that models with 2 – 3 sinusoids, which simulate active regions across multiple differentially rotating latitudes, do not significantly improve the rotational fits. The linear trend is included to approximate active regions of varying strength rotating into view or changes in emission strength during a rotation. A single sinusoid cannot account for such changes. The rotational variability function has the form

$$F = A_0 \sin((t - T_0)2\pi/P_{\text{rot}}) + bt + C \quad (1)$$

where A_0 is the amplitude, T_0 is the time offset from the date of the first observation, P_{rot} is the rotation period, and $bt + C$ is a linear trend. The fits are performed using a Markov chain Monte Carlo procedure based on the algorithm from Goodman & Weare (2010) (see also Foreman-Mackey et al. 2012). With the exception of the rotation period, non-restrictive uniform priors are set for all of the parameters. The values allowed for the rotation period are uniformly restricted to $11.0 \leq P_{\text{rot}} \leq 16.5$ days according to the measurements from Fares et al. (2017). This allows us to account for rotating active regions at latitudes other than the equator, effectively simulating differential rotation but with the constraint that only one latitude is producing the variations. We take the median of the marginalized posterior distributions as the best-fit value for each parameter. The best-fitting rotational curve is then subtracted from the raw residual flux curve, which allows the resulting

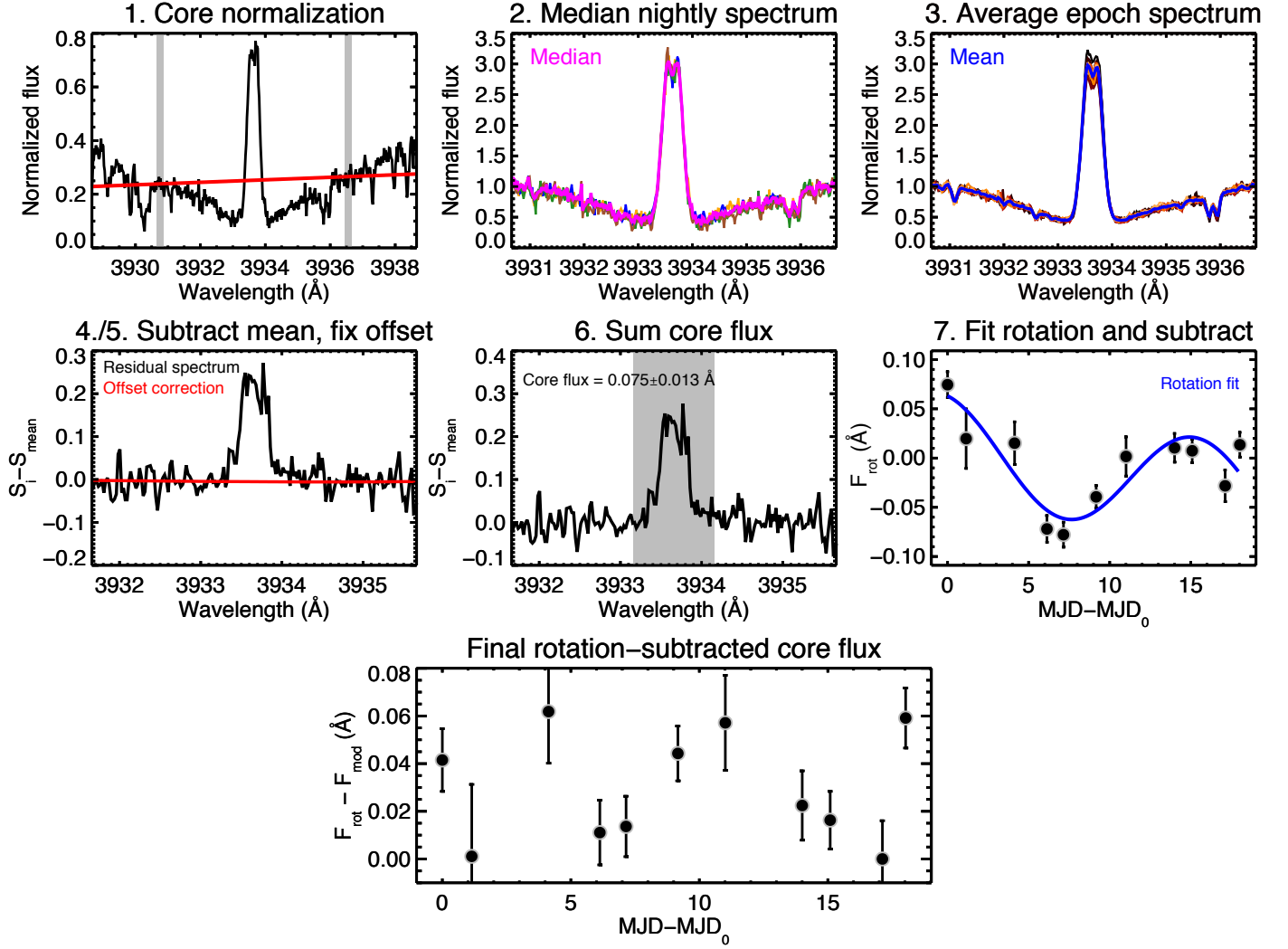


Figure 1. Illustration of the step-by-step procedure for deriving the residual Ca II K flux. The data from 2013 August are used as the examples.

variations to be examined for potential SPI signatures (e.g., bottom panel in Figure 1).

The rotational parameters and their 68% confidence intervals are given in Table 2. One interesting result to note about the best-fit periods is their non-equatorial values. The rotation periods derived here, combined with the differential rotation measurements of Fares et al. (2010, 2017), suggest active regions located at latitudes of $\approx 40^\circ - 80^\circ$. This is consistent with the active region latitudes found by Lanza et al. (2011) while modeling spots and activity-induced radial velocity variations.

3. RESULTS

In this section we present the results of the Ca II K flux analysis and the search for periodicity in the residual fluxes for each epoch.

Table 2. Stellar rotation fit parameters from Equation 1

Epoch	P_{rot}		T_0		
	(days)	A_0	(days)	C	b
(1)	(2)	(3)	(4)	(5)	(6)
2006 Jun	$14.9^{+1.1}_{-2.5}$	$0.055^{+0.018}_{-0.020}$	$1.43^{+0.96}_{-0.82}$	$-0.057^{+0.027}_{-0.027}$	$0.010^{+0.005}_{-0.005}$
2007 Jul	$14.2^{+1.5}_{-1.9}$	$0.173^{+0.049}_{-0.045}$	$8.66^{+1.54}_{-1.94}$	$0.120^{+0.067}_{-0.073}$	$-0.023^{+0.013}_{-0.012}$
2008 Jul	$13.9^{+1.8}_{-2.6}$	$0.046^{+0.023}_{-0.014}$	$2.70^{+7.16}_{-1.07}$	$0.074^{+0.024}_{-0.054}$	$-0.016^{+0.009}_{-0.004}$
2013 Aug	$15.9^{+0.4}_{-0.6}$	$0.052^{+0.005}_{-0.005}$	$4.64^{+0.53}_{-0.66}$	$0.012^{+0.009}_{-0.008}$	$-0.002^{+0.001}_{-0.001}$
2013 Sep	$15.8^{+0.4}_{-4.6}$	$0.028^{+0.004}_{-0.002}$	$6.82^{+0.66}_{-0.87}$	$-0.026^{+0.011}_{-0.008}$	$0.001^{+0.001}_{-0.001}$
2015 Sep	$13.8^{+1.4}_{-1.0}$	$0.206^{+0.040}_{-0.026}$	$0.50^{+0.81}_{-0.38}$	$-0.192^{+0.038}_{-0.068}$	$0.028^{+0.010}_{-0.007}$

3.1. Mean Ca II K fluxes and nightly variations

The mean Ca II K spectrum for each epoch is shown in the top row of Figure 2. The 2015 July data shows the highest activity level, i.e., the largest core flux, and 2007 June is the lowest. Also shown in Figure 2 are the mean absolute deviation (MAD) profiles for each epoch (bottom row), which is a measure of how much the Ca II K line core varies across the epoch. The MAD profile is constructed by taking the mean of the absolute value of the nightly residual profiles. Note that epochs with the most Ca II K core emission do not necessarily show the strongest MAD profiles.

The spectra show a significant amount of nightly variability. Figure 3 shows the integrated residual Ca II K core flux for all of the individual exposures. The intra-night variability is large on some nights, spanning almost the full range of residual core flux for the entire epoch, e.g., the fourth night (purple symbols) of 2006 June. The intra-night variability also changes from night to night and epoch to epoch, highlighting the dramatic nature of the constantly evolving active regions on the surface of HD 189733.

We also examine how the intra-night variations relate to the overall Ca II K emission levels. The residual core flux for each epoch is calculated by integrating the spectra in the top row of Figure 2 across a 1 Å band centered on Ca II K. To quantify the magnitude of the intra-night variability, we take the interquartile of the residual fluxes in Figure 3, hereafter referred to as IQR, for a single night. We then average these nightly IQR values to find the mean IQR for the epoch. The IQR uncertainties are the standard deviation of the mean for that epoch. The mean IQR values are shown as a function of the Ca II K core flux in the left panel of Figure 4. We find no trend for the IQR as a function of Ca II K core flux.

There is, however, a correlation between mean IQR and the integrated MAD flux, which is shown in the right panel of Figure 4: epochs with larger MAD fluxes tend to exhibit larger IQR values. In other words, epochs with greater average Ca II K core flux variations across the entire epoch (e.g., from rotational and any orbital modulation) are the same epochs which show the largest average intra-night variability. This suggests that average night-to-night variations are a better proxy for how active the star is on hours-long timescales than the absolute core flux level of the epoch’s mean Ca II K spectrum.

3.2. Periodic variations in the Ca II K residuals

The Ca II K residual profiles and flux as a function of time are shown in Figure 5. The rotation fits from Section 2.2 are over plotted in the middle rows and the residual flux minus the rotation fits are given in the bottom rows. Uncertainties for the residual flux are derived by summing in quadrature the normalized flux uncertainties of the residual spectrum. Note that the normalized flux uncertainty is estimated from the spectrum ad-

acent to the line core, where the signal-to-noise is $\approx 2\times$ lower than in the line core HD 189733 (see Figure 2). Thus the residual flux uncertainties are conservative.

We employed the Lafler-Kinman statistic to search for periodicity in the rotation-subtracted Ca II K residuals in Figure 5. The Lafler-Kinman (LK) statistic is a non-parametric string-length method for evaluating periodicity within time series data (Clarke 2002). Clarke (2002) explored the behavior of the LK statistic, which we refer to as $T(P)$ (see equation 3 of Clarke 2002), as a function of the number of time series points N and the signal-to-noise ratio (SNR) of the data. They derived values of $T(P)$ which describe the maximum value for which a test period can be considered significant at some confidence level. These maximum $T(P)$ values are a function of N and the SNR. Here we interpolated among the 90%, 95%, and 99% $T(P)$ values from Table 1 of Clarke (2002) for the appropriate values of N and SNR of our data. Note that for small N there is sometimes no value of $T(P)$ corresponding to some confidence level.

We performed the period search within the range $1 \text{ day} \leq P \leq \max(T-T_0)$ where $T-T_0$ is the number of nights spanning the entire epoch. We initially chose a period resolution of 0.01 days. Calculating $T(P)$ requires ordering the data by increasing phase. We use the inferior conjunction (i.e., mid-transit) BJD $T_0 = 2453955.525511$ (Baluev et al. 2015) for the phase calculations. The $T(P)$ values for each epoch are shown in Figure 6. The red, orange, and purple lines mark the 90%, 95%, and 99% confidence values of $T(P)$ for each case. Note that the small number of points and poor SNR for 2007 June ($N = 8$, $\text{SNR} \approx 0.7$) makes it impossible to assign a confidence of $\geq 90\%$ to any value of $T(P)$; thus no significant periods are reported for this epoch. The 2013 September is the only data set for which a 99% confidence value of $T(P)$ can be determined.

It is important to reiterate that the confidence levels do not imply that some period with a low $T(P)$ value is a physical period; they instead give the probability with which that period is detected in the data set. Thus it is possible to have spurious periods with $T(P)$ values below some high confidence level. Evaluation of the likelihood that a similarly significant period would be detected by chance must be performed separately, which we do in the next section.

3.3. Statistical tests of detected periods

In order to determine the uncertainties of the lowest $T(P)$ periods in Figure 6, we adopted the procedure from Fernie (1989) (see also Kwee & van Woerden 1956). The procedure involves finely sampling the period space near the $T(P)$ minimum and fitting a parabola to the $T(P)$ values in the vicinity. The quadratic coefficients are then used to calculate the period and its uncertainty. The zoomed-in period- $T(P)$ space is shown in Figure 7 and the best-fit periods and associated uncertainties are

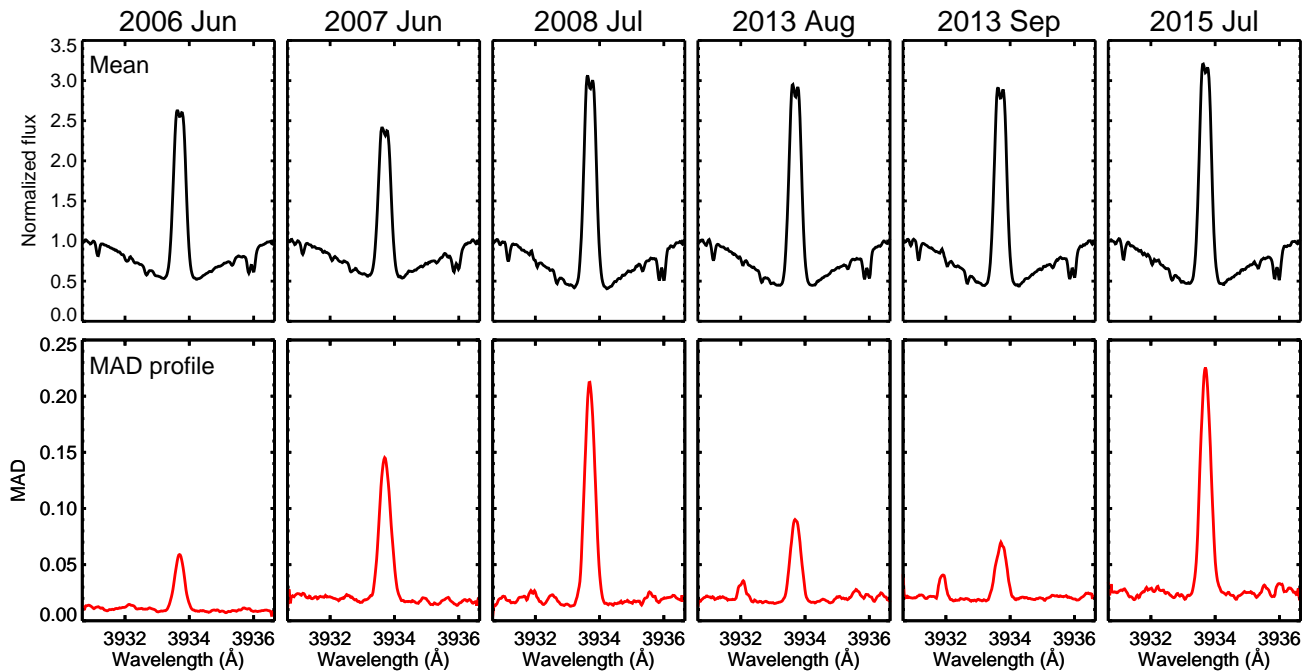


Figure 2. Master Ca II K profiles for each epoch (top row) and smoothed mean absolute deviation (MAD) profiles of the Ca II K line core (bottom row). The blips at ≈ 3932 Å in the 2008 July and 2013 August and September epochs are the result of imperfect removal of a bad pixel in the NARVAL data. Epochs with the largest Ca II K emission do not necessarily show larger MAD profiles.

Table 3. Lowest $T(P)$ periods and their uncertainties

Observation epoch	Period		
	$\min(T(P))$	(days)	Detection significance
(1)	(2)	(3)	(4)
2006 Jun	0.19	1.26 ± 0.04	> 90%
2007 Jun
2008 Jul	0.37
2013 Aug	0.11	2.29 ± 0.04	> 95%
2013 Sep	0.19	$6.20 \pm .17$	> 99%
2015 Jul	0.43

given in Table 3. The 2008 July and 2015 July epochs show no smooth minima and thus no reliable fits. We reject these low $T(P)$ values as spurious. The 2006 June, 2013 August, and 2013 September data display reasonable minima, although the 2013 September space is fairly broad. The lowest $T(P)$ value found for any epoch is $T(P) = 0.11$ for 2013 August. The best-fit period of 2.29 ± 0.04 days for 2013 August is consistent at $\approx 2\sigma$ with the planet’s orbital period of $P_{\text{orb}} \approx 2.219$ days.

Figure 8 shows the Ca II K residuals phased to the best-fit periods from Table 3 for 2006 June, 2013 August, and 2013 September. The 2006 June and 2013 August

residuals have very similar forms, e.g., truncated sine curves, with peak fluxes near $\phi \approx 0.7 - 0.8$ for 2006 June and $\phi \approx 0.0 - 0.1$ for 2013 August. The 2013 September residuals show a gradual increase in flux and then a sharp drop near $\phi \approx 0.5$.

In order to test the significance of the best-fit periods, we performed statistical assessments of how likely it is to obtain a set of residual fluxes with a similar or better value of $T(P)$. In other words, how likely is it to measure $T(P) \leq \min(T(P))$ from a randomly generated set of residual fluxes? To do this we looked at three cases: 1. normally distributed fluxes with standard deviation and mean equal to the measured fluxes; 2. uniformly distributed fluxes bounded by the minimum and maximum of the measured values; and 3. randomly re-ordered values of the measured fluxes. The observation dates are kept constant. For each case we generated $N = 5000$ random flux vectors and performed the same $T(P)$ analysis for each vector as was done for the observed data. We then took the minimum $T(P)$ value from the period analysis and compared all of these $T(P)$ values to the observed minimum $T(P)$ value. The p -value for each case is then the fraction of repetitions which produce $\min(T(P)) \leq \min(T(P))_{\text{obs}}$.

The $T(P)$ histograms and derived p -values for the epochs with significant periods are shown in Figure 9 and the p -values are summarized in Table 4. The 2006

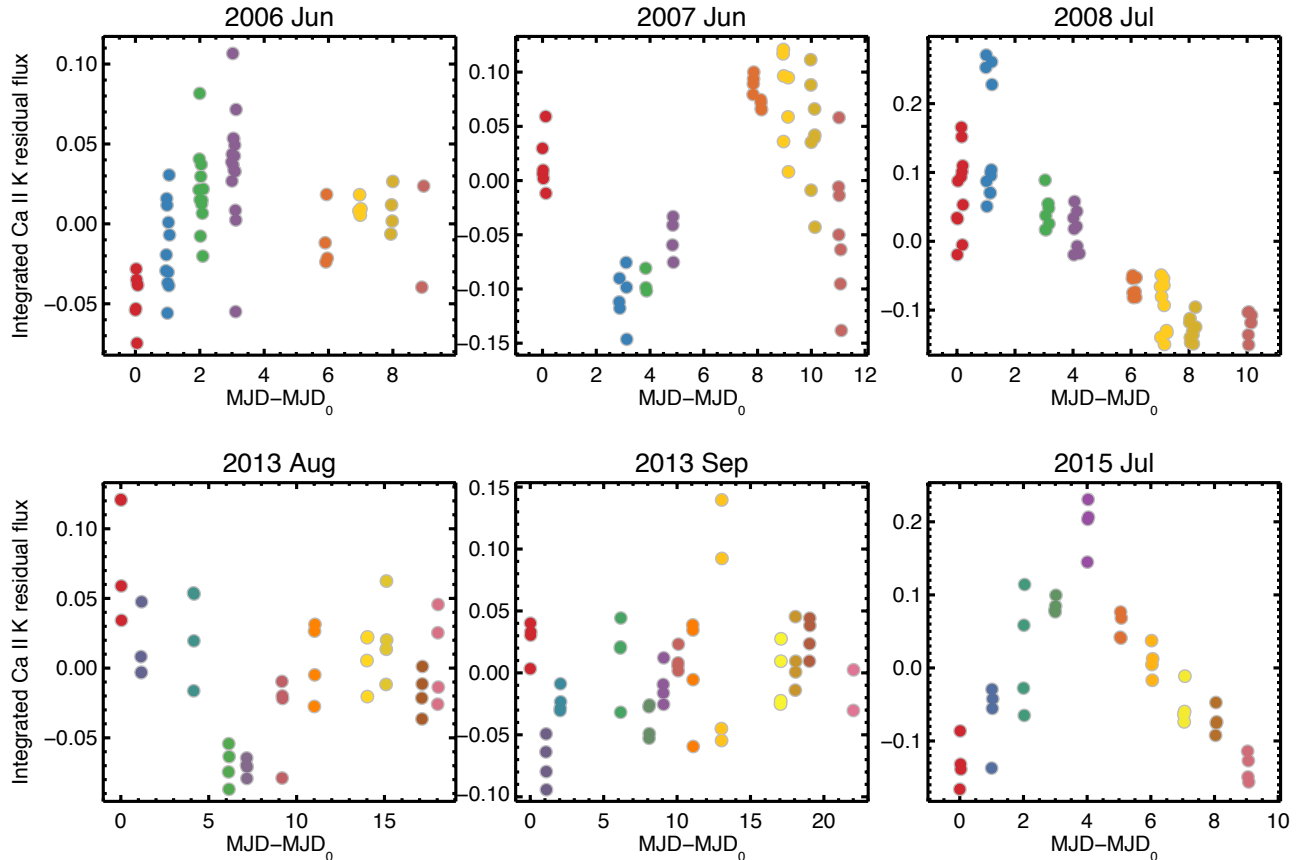


Figure 3. Integrated residual Ca II K core flux for individual spectra as a function of time. Spectra from the same night are plotted with the same color. Note the different y-axis scaling for each epoch. The spectra show large nightly variations in the Ca II K core flux and the magnitude of the variations changes night to night and epoch to epoch.

June epoch has fairly large p -values for all of the test methods, suggesting that the detected period is not robust. This is mainly the result of the small number of observations ($N = 8$). Although not as high, the 2013 September epoch did not produce a p -value less than 1% and did particularly poorly in the Uniform test case, with $p = 0.052$. The most robust signal by far is from the 2013 August data: $p < 0.01$ in all of the test cases, providing evidence that $< 1\%$ of random residual flux measurements will result in a value of $T(P)$ as low as that measured from the data. We thus consider the 2013 August signal to be the only significant detection and do not further discuss the marginal cases of 2006 June and 2013 September.

4. DISCUSSION

We analyzed periodicity in the rotation-subtracted Ca II K residual flux for six observations epochs of HD 189733. We found one statistically robust period: $P = 2.29 \pm 0.04$ days for the 2013 August epoch. This period is consistent with the orbital period of HD 189733 b.

Table 4. Minimum $T(P)$ and statistical test p -values

Observation epochs	min($T(P)$)	p -values				Mean
		Normal	Uniform	Reordered		
(1)	(2)	(3)	(4)	(5)	(6)	
2006 Jun	0.19	0.043	0.084	0.354	0.160	
2013 Aug	0.11	0.001	0.003	0.006	0.003	
2013 Sep	0.19	0.020	0.052	0.010	0.027	

Magnetic SPI signals are predicted to be modulated at the planet’s orbital or beat period, where the planet continuously excites Alfvén waves (Preusse et al. 2006; Kopp et al. 2011; Strugarek et al. 2016) or experiences reconnection events with the stellar magnetic field as it moves through the magnetosphere (Lanza et al. 2011, 2012). Thus the detection of a robust period very near the planet’s orbital period is an indication that we are in fact measuring the effects of magnetic SPI in the system.

Besides the evidence of the SPI signal itself, the 2013 August variations are interesting for a variety of reasons.

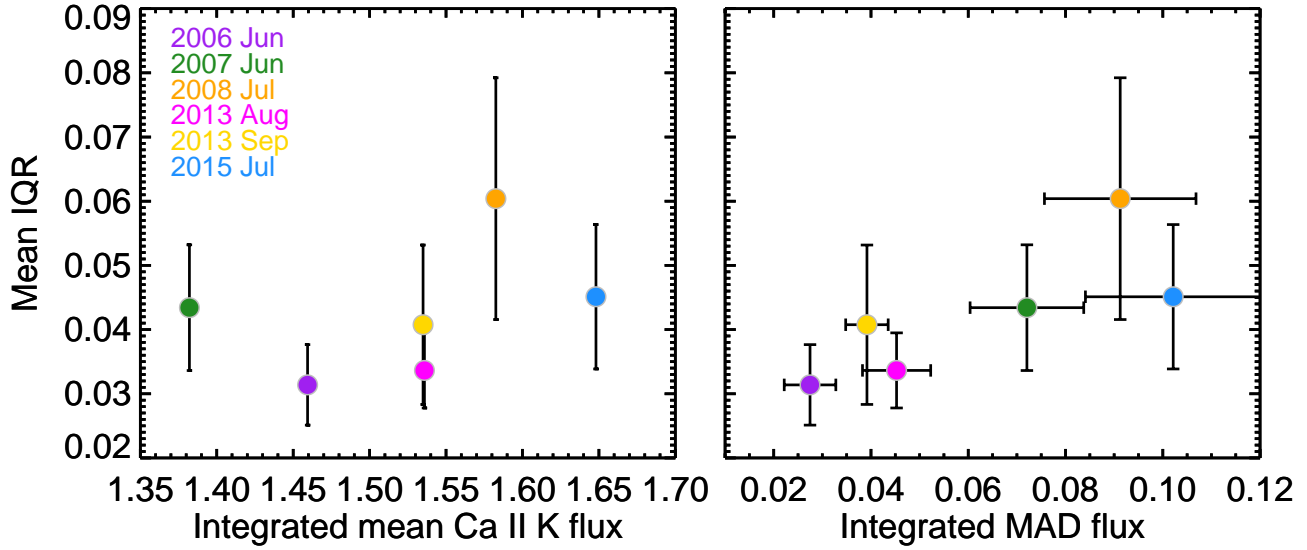


Figure 4. Mean nightly interquartile residual fluxes (IQR) versus the integrated Ca II K core flux (left panel) and integrated MAD flux (right panel) for each epoch. The uncertainties for the Ca II K core fluxes are smaller than the plot symbols. There is no noticeable trend with Ca II K core flux, suggesting that HD 189733 exhibits stochastic nightly variability at a similar magnitude regardless of the absolute activity level. However, a trend can be seen in the right panel: epochs with overall larger changes in Ca II K core flux, i.e., larger MAD fluxes, tend to show greater intra-night variability, or IQR values.

The second lowest $T(P)$ value in Figure 7 is at 2.22 days, almost exactly the orbital period of HD 189733 b ($P_{\text{orb}} = 2.218575$ days; Baluev et al. 2015). The rotationally-subtracted Ca II K residuals phased to the planet’s orbital period are shown in Figure 10. If we assume that the signal is strongest when the projected area of the emitting region is largest, i.e., when the SPI hot spot crosses the line-of-sight, this corresponds to a phase lead of $\Delta\phi \approx 40^\circ$ ahead of the planet. This is roughly consistent with the phase lead of $\Delta\phi = 53^\circ$ for HD 189733 found by Lanza et al. (2012) for a model assuming a non-linear force-free stellar magnetic field.

Fares et al. (2017) calculated the stellar magnetic field strength and configuration of HD 189733 for all of the epochs examined here, with the exception of the 2006 June epoch, which was presented by Moutou et al. (2007). They find that the stellar field changes significantly, even on timescales of a few rotation periods. They extrapolate the stellar field strength to the planet’s orbital distance and find average field strengths of $B_*^{\text{orb}} = 16, 23, 39, 31,$ and 18 mG for the epochs of 2007 June, 2008 July, 2013 August, 2013 September, and 2015 September, respectively (see Table 4 of Fares et al. 2017). We note that although no field extrapolation exists for the 2006 June epoch, the surface field strength is low ($B_* = 18$ G), ruling out a large field strength at the planet’s orbit. Fares et al. (2017) also show that the planet can move through drastically different coronal conditions over a single orbit (see also Llama et al. 2013).

The B_*^{orb} value for 2013 August may offer a clue as to why this epoch shows evidence for magnetic SPI: the power in magnetic SPI scales as $P \propto v_{\text{rel}} R_p^2 B_p^{2/3} B_*^{4/3}$ (e.g., Lanza 2009; Lanza et al. 2012) where v_{rel} is the relative velocity between the planet and stellar magnetic field lines, R_p is the planet’s radius and B_p is the planetary magnetic field, suggesting that a larger stellar magnetic field strength at the planet’s orbit should produce stronger SPI emission. Assuming the other system parameters are constant, the value of B_*^{orb} for 2013 August implies that the available power for magnetic SPI is $\approx 2.3\times$ greater on average than for the other epochs. Thus the larger magnetic field strength may be an important contributor to the observed SPI signature.

5. SUMMARY AND CONCLUSIONS

We analyzed six archival high resolution Ca II K data sets (58 total nights) for the hot Jupiter system HD 189733 in order to search for signatures of magnetic star-planet interactions. After removing the rotational modulations we find statistically significant ($\bar{p} = 0.003$; $> 99\%$) variations for the 2013 August data set at a period of 2.29 ± 0.04 days, consistent with the orbital period of HD 189733 b; none of the other epochs show variations with a significance greater than $\approx 95\%$, which is not unexpected given the high activity level of HD 189733 and the short timescales over which the stellar magnetic field changes strength and morphology (Fares et al. 2017).

The SPI signal reported here has characteristics that are consistent with the non-linear force-free magnetic

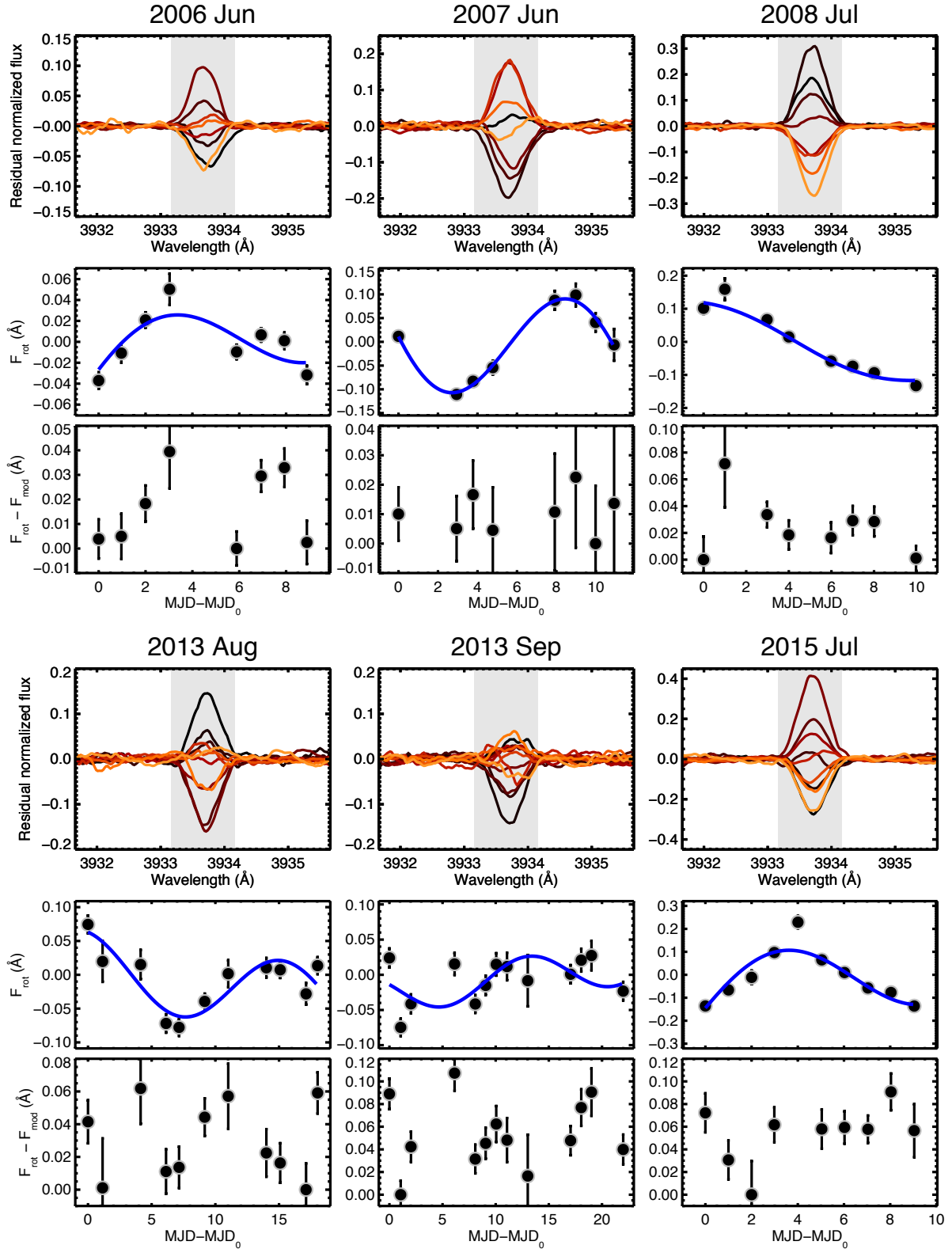


Figure 5. Residual Ca II K profiles (top rows), raw residual flux curves (middle rows), and residual flux with rotational modulations removed ($F_{\text{rot}} - F_{\text{mod}}$). The residual line profiles are smoothed for clarity. The gray shaded regions indicate the residual flux integration range. Spectrum colors move from black for earlier dates to yellow-orange for later dates. The blue lines are the rotational fits to the raw flux curves. Note that the y-axis scaling is different for each epoch and that the $F_{\text{rot}} - F_{\text{mod}}$ values have been shifted so that the lowest value is zero.

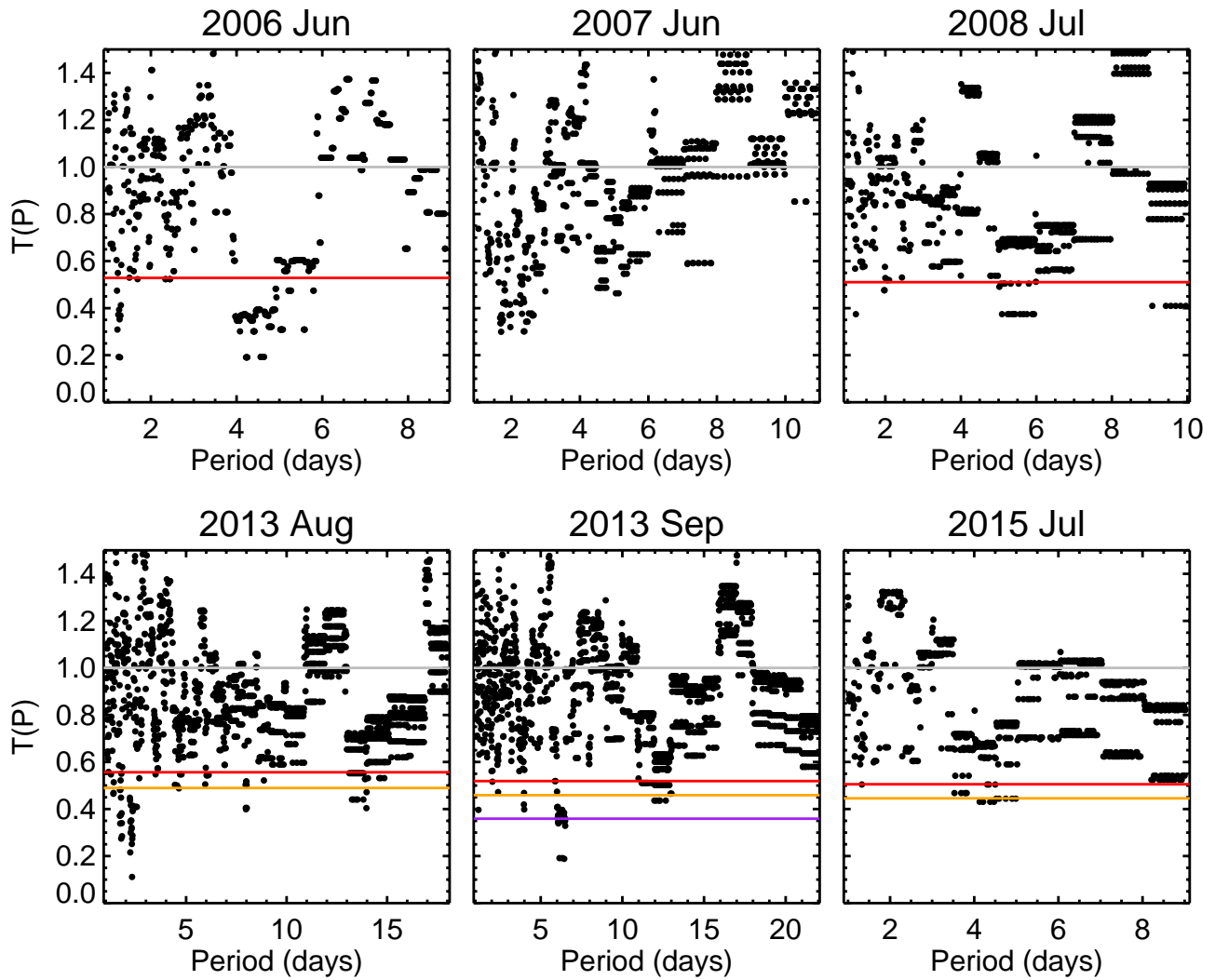


Figure 6. $T(P)$ as a function of period for each epoch. The $T(P)$ values indicating a period at 90%, 95%, and 99% confidence are marked with the horizontal red, orange, and purple lines, respectively. No periods with confidence greater than 90% can be determined for the 2006 June and 2008 July epochs, while no periods with significance at $> 90\%$ can be determined at all for the 2007 June epoch.

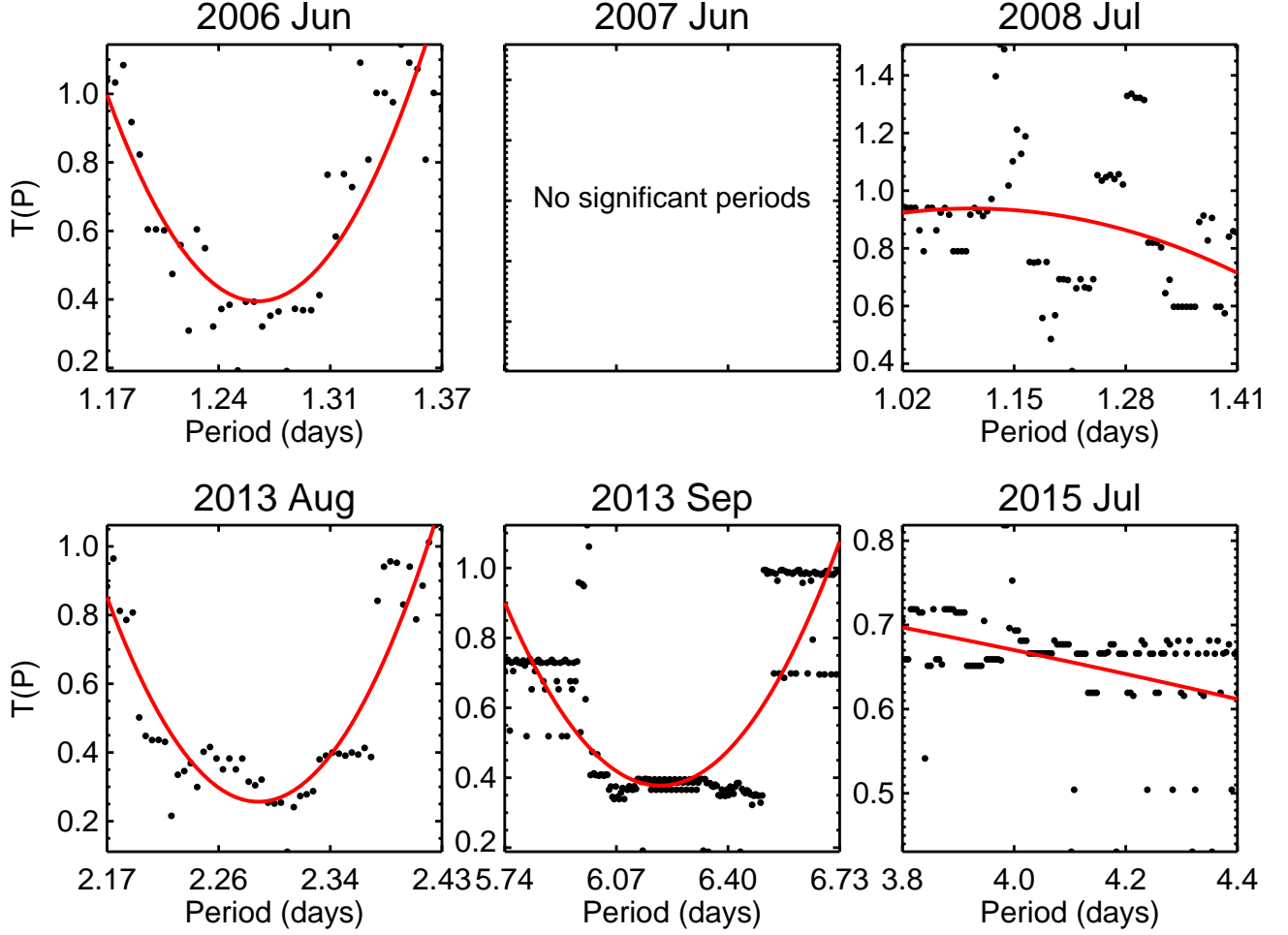


Figure 7. $T(P)$ values zoomed in on the lowest $T(P)$ values from Figure 6. The period space around the minima are explored with a resolution of 0.005 days. The best-fit parabola to the $T(P)$ minima are over-plotted in red. Note that the y-axis scale is different for each epoch. Only the epochs of 2006 June and 2013 August show well-defined minima; 2013 September has a much broader minimum and is weakly described by a parabolic fit. The best-fit period for 2013 August is consistent with the planet’s orbital period.

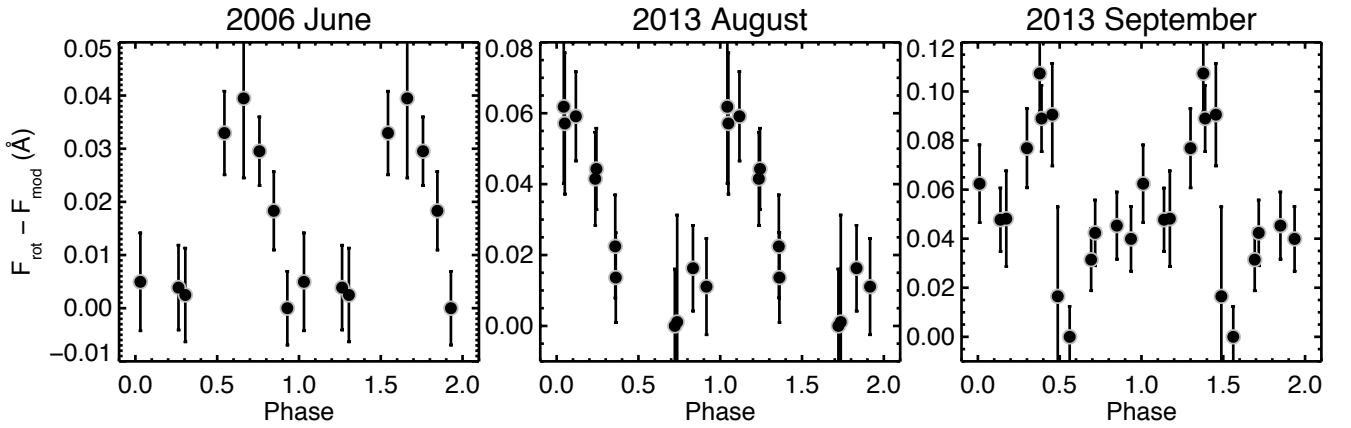


Figure 8. Residual Ca II K fluxes, with rotational modulations removed, phased to the best-fit periods from Table 3. The data is repeated in phase for display purposes. The 2006 June and 2013 August residuals show peak fluxes at approximately the same phase.

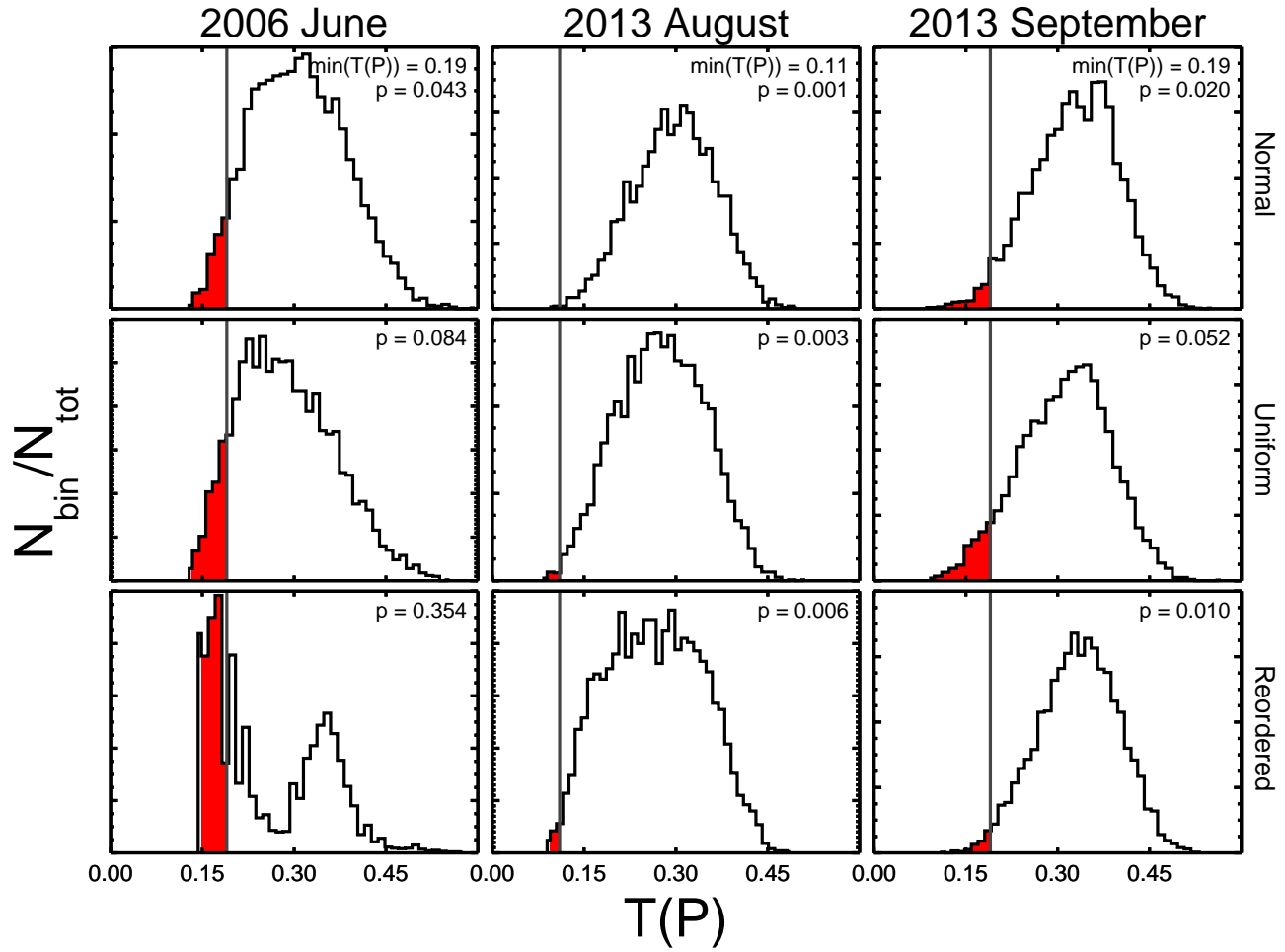


Figure 9. $T(P)$ histograms for random flux tests. The rows represent the different methods: random draws from a normal distribution (first row), random draws from a uniform distribution (second row), and randomly reordered flux vectors (third row). Red filled regions show $T(P) \leq \min(T(P))_{\text{obs}}$. The $\min(T(P))_{\text{obs}}$ value is marked with a vertical gray line and labeled in the upper-right of the top panels. The p -values are also given for each test. The only epoch with a consistently low p -value is 2013 August, suggesting a robust period detection.

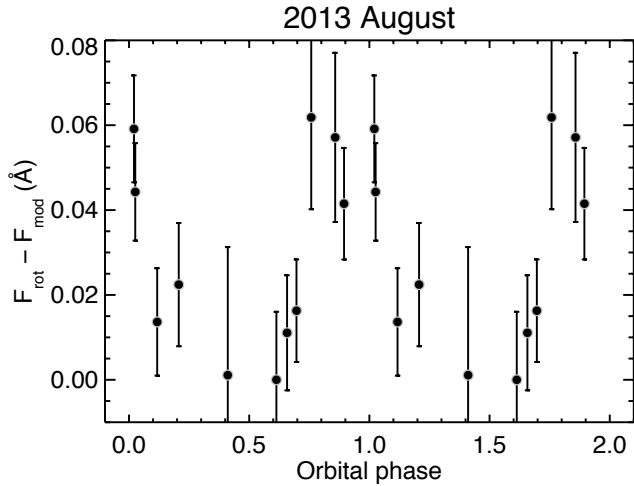


Figure 10. Rotationally-subtracted Ca II K residual fluxes as a function of the precise orbital period of HD 189733 b. The average phase of the maximum fluxes is ≈ 0.9 , which translates to a phase lead by the SPI hotspot of $\Delta\phi \approx 40^\circ$.

SPI model suggested by Lanza et al. (2012), specifically the phase offset of $\Delta\phi \approx 40^\circ$ between the planet and magnetic interaction. The absence of SPI signals in the

majority of the analyzed epochs illustrates the fickle nature of these signals (e.g., Shkolnik et al. 2008), which depend on the magnetic field strength and configuration of the host star at the time of observations and are likely obscured, even when present, to some extent by stochastic stellar variability. Our results reinforce the need for rigorous monitoring of any potential SPI systems over many planetary orbits in order to maximize the opportunity of catching the star and planet in a favorable configuration.

Acknowledgments: We thank the referee for their consideration of the manuscript, which helped improve the analysis and results. We thank Gordon Walker and David Bohlender for their valuable input. This work is supported by NASA Origins of the Solar System grant No. NNX13AH79G (PI: E.L.S.). This work has in part been carried out in the frame of the National Centre for Competence in Research PlanetS supported by the Swiss National Science Foundation (SNSF). V.B. acknowledges the financial support of the SNSF. This project has received funding from the European Research Council (ERC) under the European Union’s Horizon 2020 research and innovation programme (project FOUR ACES; grant agreement No 724427). This work has made use of NASA’s Astrophysics Data System.

REFERENCES

- Baluev, R. V., Sokov, E. N., Shaidulin, V. Sh., et al. 2015, *MNRAS*, 451, 3101
- Bouchy, F., Udry, S., Mayor, M., et al. 2005, *A&A*, 444, L15
- Cauley, P. W., Redfield, S., & Jensen, A. G. 2017, *AJ*, 153, 185
- Cegla, H. M., Lovis, C., Bourrier, V., et al. 2016, *A&A*, 588, 127
- Clarke, D. 2002, *A&A*, 386, 763
- Cohen, O., Kashyap, V. L., Drake, J. J., Sokolov, I. V., Garraffo, C., & Gombosi, T. I. 2011, *ApJ*, 733, 67
- Cranmer, S., & Saar, S. 2007, pre-print (arXiv:astro-ph/0702530)
- Cuntz, M., Saar, S. H., & Musielak, Z. E. 2000, *ApJ*, 533, L151
- Donati, J.-F., Semel, M., Carter, B. D., Rees, D. E., & Cameron, A. C. 1997, *MNRAS*, 291, 658
- Fares, R., Donati, J.-F., Moutou, C., et al. 2010, *MNRAS*, 406, 409
- Fares, R., Moutou, C., Donati, J.-F., et al. 2013, *MNRAS*, 435, 1451
- Fares, R., Bourrier, V., Vidotto, A. A., et al. 2017, *MNRAS*, 471, 1246
- Fernie, J. D. 1989, *PASP*, 101, 225
- Foreman-Mackey, D., Hogg, D. W., Lang, D., & Goodman, J. 2012, arXiv:1202.3665
- Goodman, J., & Weare, J. 2010, *CAMCS*, 5, 65
- Hébrard, G., & Lecavelier Des Etangs, A. 2006, *A&A*, 445, 341
- Kopp, A., Schilp, S., & Preusse, S. 2011, *ApJ*, 729, 116
- Kwee, K. K., & van Woerden, H. 1956, *Bull. Astron. Inst. Netherlands*, 12, 327
- Lanza, A. F. 2009, *A&A*, 505, 339
- Lanza, A. F. 2010, *A&A*, 512, A77
- Lanza, A. F., Boisse, I., Bouchy, F., et al. 2011, *A&A*, 533, A44
- Lanza, A. F. 2012, *A&A*, 544, A23
- Lazio, T. J. W., Shkolnik, E., Hallinan, G., et al. 2016, *Planetary Magnetic Fields: Planetary interiors and habitability*, final report prepared by the Keck Institute of Space Studies
- Llama, J., Vidotto, A. A., Jardine, M., et al. 2013, *MNRAS*, 436, 2179
- Moutou, C., Donati, J.-F., Savalle, R., et al. 2007, *A&A*, 473, 651
- Petit, P., Louge, T., Théado, S., et al. 2014, *PASP*, 126, 939
- Pillitteri, I., Gunther H.M., Wolk S.J., Kashyap V.L., & Cohen, O. 2011, *ApJ*, 741, 18

- Pillitteri, I., Wolk, S. J., Lopez-Santiago, J., et al. 2014, *ApJ*, 785, 145
- Pillitteri, I., Maggio, A., Micela, G., et al. 2015, *ApJ*, 805, 52
- Poppenhaeger, K., & Wolk, S. J. 2014, *A&A*, 565, 1
- Preusse, S., Kopp, A., Büchner, J., & Mutschmann, U. 2006, *A&A*, 460, 317
- Shkolnik, E., Walker, G. A. H., & Bohlender, D. A. 2003, *ApJ*, 587, 1092
- Shkolnik, E., Walker, G. A. H., Bohlender, D. A., Gu, P.-G., & Kürster, M. 2005, *ApJ*, 622, 1075
- Shkolnik, E., Bohlender, D. A., Walker, G. A. H., & Collier Cameron, A. 2008, *ApJ*, 676, 628
- Shkolnik, E. L., & Llama, J. 2017, Signatures of Star-Planet Interactions. In: Deeg H., Belmonte J. (eds) *Handbook of Exoplanets*. Springer, Cham
- Strugarek, A., Brun, A. S., Matt, S. P., & Réville, V. 2015, *ApJ*, 815, 111
- Strugarek, A. 2016, *ApJ*, 833, 140